A Noise Subspace Projection Approach to Target Signature Detection and Extraction in an Unknown Background for Hyperspectral Images

Te-Ming Tu, Chin-Hsing Chen, and Chein-I Chang, *Senior Member, IEEE*

***Abstract*— A noise subspace projection (NSP) approach to extraction and subpixel detection of target signatures in an unknown background is presented. The proposed NSP approach is derived from a recently developed subspace orthogonal projection (OSP) method and can be shown to be approximated by an adaptive filter with the optimal weight given by the Wiener–Hopf equation. As a result, the operator resulting from the NSP approach can be used as an OSP operator for scene classification and subpixel detection, on one hand, and also implemented as an adaptive filter, on the other. These advantages make the NSP approach very attractive in practical applications. In particular, the NSP operator takes advantage of the noise subspace projection to prevent from inverting correlation matrices, as required by an adaptive filter.**

***Index Terms*—Adaptive filter, hyperspectral image, noise subspace projection (NSP), orthogonal subspace projection (OSP).**

I. Introduction

HYPERSPECTRAL imagery provides more information than multispectral imagery in the sense that the spectral resolution of the former is much better than that of the latter. For example, an airborne visible/infrared imaging spectrometer (AVIRIS) image is acquired by 224 bands, while a multispectral image generally requires only five to seven bands. In particular, when a scene covers distinct materials more than the number of spectral bands used by multispectral imagery, the multispectral capability of distinguishing image endmembers degrades significantly, and in this case, we must rely on hyperspectral imagery, which offers the spectral resolution <10 nm and expands detection and classification activities to targets unresolved in multispectral images [1].

In this paper, the main focus is the detection of target signatures in an unknown background. The considered detection problem is not quite the same as ones encountered in image processing. Since the targets of interest are generally smaller than the spatial resolution of hyperspectral images (e.g., pixel resolution 20 m $\times$ 20 m), it is necessary to develop subpixel detection techniques for this purpose. An approach recently developed by Harsanyi and Chang [2] called the orthogonal subspace projection (OSP) method has demonstrated a promising application to subpixel detection problems, but requires knowledge of signatures and background. Some related works in the comparative analysis of subspace projection methods can be found in [3]–[7].

In [8], the OSP method is further extended and designed for subpixel detection and classification in an unknown background, where the developed OSP-based subpixel technique, called low probability detection (LPD), was used to detect targets appearing in an image with low probability. A low probability target is defined as a target that occurs in very few pixels in the image; thus, it can be viewed as an insignificant target. In most cases, such insignificant targets are very important, but generally overlooked or discarded, such as detecting a tank in a field. The LPD approach not only can detect low probability targets, but also assumes no prior knowledge about the background. It was proved to be very effective and practically useful. Another approach proposed in [8], called the constrained energy minimization (CEM) method, was to apply the concept of linearly constrained adaptive beamforming to the case where the exact knowledge of signatures and background is not known *a priori*. Under these circumstances, an adaptive beamforming-type classifier and subpixel detector were developed to complement the OSP and LPD methods. In analogy to the CEM method, an adaptive method for optimal jammer suppression in adaptive array processing by using the orthogonal projection was also suggested in [9] and shown to be superior to the commonly used sample correlation matrix inversion (SMI) algorithm.

Motivated by the ideas in [2]–[9], a noise subspace projection (NSP) approach to target signature detection and extraction in an unknown background is proposed. It originates from the concept of orthogonal subspace projection (OSP) [2] and is developed in conjunction with the idea in [9]. In particular, it is shown in this paper that the operator resulting from the NSP approach can be approximated by an adaptive filter with the optimal weight specified by the celebrated Wiener–Hopf equation, provided that the total energy of signatures is large compared to the noise energy and, particularly, for the case where the target signature is weak. As a result, the NSP operator can be implemented as an adaptive filter without need for specific knowledge of signatures except the correlation

Manuscript received August 8, 1995; revised September 16, 1996. This work was supported by the National Science Council under Grants NSC 85-2213-E-006-066 and NSC 84-2213-E-006-086.

T.-M. Tu is with the Department of Electrical Engineering, Chung Cheng Institute of Technology, Tahsi, Taoyuan 33509, Taiwan, R.O.C. (e-mail: tutm@cc04.ccit.edu.tw).

C.-H. Chen is with the Department of Electrical Engineering, National Cheng Kung University, Tainan 70101, Taiwan, R.O.C.

C.-I. Chang is with the Remote Sensing Signal and Image Processing Laboratory, Department of Computer Science and Electrical Engineering, University of Maryland-Baltimore County, Baltimore, MD 21228-5398 USA (e-mail: cchang@umbc2.umbc.edu).

Publisher Item Identifier S 0196-2892(98)00036-9.

matrix. On the other hand, the NSP operator can be also used as an OSP-based interference rejecter that eliminates the undesired signatures/interferences while preserving the desired target signatures. Since the OSP uses the spectral decomposition of a covariance matrix to design an orthogonal projection interference rejecter, the matrix inversion is done by finding the inverses of eigenvalues. Therefore, direct matrix inversion is not necessary in the NSP operator. This is a significant advantage over adaptive filters, especially, when the dimensionality of the correlation matrix is very high, e.g., hyperspectral image data.

This paper is organized as follows. Section II describes the linear mixture model for multispectral/hyperspectral imagery. Section III reviews three widely used estimation techniques used in adaptive filtering theory, based on minimum mean-squared error (MMSE) and maximum signal-to-interference/noise (MSINR) ratio. Section IV derives the relationship between inverses of two correlation matrices of which one contains the desired signatures and the other does not. Section V shows that the OSP method recently developed by Harsanyi and Chang in [2] can be approximated by an adaptive filter solved by the Wiener–Hopf equation when the energy of signatures is large compared to noise energy. Section VI presents a noise subspace projection approach, which is derived from the OSP method and Wiener–Hopf equation and can be used for subpixel detection and extraction in an unknown background. Section VII conducts three experiments to demonstrate the power and potential applications of the NSP approach. Section VIII is a brief conclusion.

Typographic Conventions: Throughout this paper, vectors are denoted by boldface lowercase letters, matrices by boldface uppercase, and transpose and matrix inverse by superscripts T, -1, respectively. $\boldsymbol{I}$ denotes the identity matrix.

II. Linear Mixture Model for Multispectral/Hyperspectral Images

Let $\boldsymbol{r}(x, y)$ be an $l \times 1$ column vector that denotes a pixel in a hyperspectral scene at spatial location (x, y), where l is the number of spectral bands. Assume that $\boldsymbol{M}$ is an $l \times p$ matrix denoted by $(\boldsymbol{m}_1, \boldsymbol{m}_2, \cdots, \boldsymbol{m}_p)$ where $\boldsymbol{m}_i$ is an $l \times 1$ column vector representing the spectral signature of ith material. We also let $\boldsymbol{\alpha}(x, y)$ be a $p \times 1$ column vector given by $[\alpha_1(x, y), \alpha_2(x, y), \cdots, \alpha_p(x, y)]^T$ where p is the number of materials and $\alpha_i(x, y)$ denotes the fraction of the ith signature present in the pixel $\boldsymbol{r}(x, y)$. A linear mixture model for the hyperspectral image pixel $\boldsymbol{r}(x, y)$ can be described by [10]–[12]

$$\boldsymbol{r}(x, y) = \boldsymbol{M}\boldsymbol{\alpha}(x, y) + \boldsymbol{n}(x, y) \tag{1}$$

where $\boldsymbol{n}(x, y)$ is an $l \times 1$ column vector representing additive-white Gaussian noise with zero mean and variance $\sigma^2\boldsymbol{I}$ and $\boldsymbol{I}$ is the $l \times l$ identity matrix.

III. Statistical Estimation of $\boldsymbol{\alpha}(x, y)$

There have been many approaches proposed to solve image classification problems for the model given by (1), such as principal components analysis, maximum likelihood, and minimum distance classification. Of particular interest is one reported in [2], which applied the concept of the OSP to (1) and resulted in an interference rejecter, which improved classification performance. Unfortunately, most currently existing classification techniques applied to multispectral/hyperspectral imagery assume complete *a priori* information about the spectral signatures, including the abundance $\boldsymbol{\alpha}(x, y)$. This is generally not true in many practical applications. Specifically, the prior knowledge of $\boldsymbol{\alpha}(x, y)$ is either very difficult to obtain or too expensive to collect. In this case, an estimate of $\boldsymbol{\alpha}(x, y)$ must be used in place of the true unknown $\boldsymbol{\alpha}(x, y)$ in (1). In what follows, three commonly used estimation techniques will be reviewed and discussed in the context of the estimation of $\boldsymbol{\alpha}(x, y)$ where $\boldsymbol{r}(x, y)$ and $\boldsymbol{\alpha}(x, y)$ are assumed to be random vectors. In order to simplify notations, the spatial location (x, y) in (1) will be suppressed throughout this paper. The first approach solves the Wiener filtering-type unconstrained problem. The second is a linearly constrained optimization technique, which is widely used in adaptive beamforming. The optimal adaptive filters derived by these two approaches are determined by the correlation matrix of $\boldsymbol{r}$. In contrast, the third approach involves maximizing the signal-to-noise/interference ratio (SNIR), as determined by two separate correlation matrices: that of the desired signature vector and that of the interference vector, which includes undesired signatures and noise [13]–[15].

A. MMSE Approaches

1) Wiener Filtering Approach: For convenience in the present discussion, we rewrite (1) in the following form:

$$\boldsymbol{r} = (r_1, r_2, \cdots, r_l)^T = \boldsymbol{M}\boldsymbol{\alpha} + \boldsymbol{n} = \boldsymbol{d}\alpha_p + \boldsymbol{U}\boldsymbol{\gamma} + \boldsymbol{n}$$

where

- $\boldsymbol{d}$ desired signature assumed without loss of generality to be the column vector $\boldsymbol{m}_p$;
- $\boldsymbol{U}$ $l \times (p-1)$ matrix given by $\boldsymbol{U} = (\boldsymbol{m}_1, \boldsymbol{m}_2, \cdots, \boldsymbol{m}_{p-1})$; and
- $\boldsymbol{\gamma}$ a vector which contains the first $(p-1)$ components of $\boldsymbol{\alpha}$, $\boldsymbol{\gamma} = (\alpha_1, \alpha_2, \cdots, \alpha_{p-1})^T$.

Let the abundance of desired signature $\boldsymbol{d}$ be denoted by α_p; α_p will be estimated by an adaptive filter, whose design is based on Wiener filtering theory. Suppose that the output y of an adaptive filter, whose weights are given by $\boldsymbol{w} = (w_1, w_2, \cdots, w_l)^T$ is expressed by $y = \sum_{k=1}^{l} w_k r_k$.

Let $\varepsilon = \alpha_p - y = \alpha_p - \boldsymbol{w}^T\boldsymbol{r}$. Then the mean square error (MSE) is given by

$$e = E[\varepsilon^2] = E[(\alpha_p - y)^2] = E[(\alpha_p - \boldsymbol{w}^T\boldsymbol{r})^2] \tag{2}$$

and the solution to minimization of (2) can be obtained by the Wiener–Hopf equation [13], [14]

$$\boldsymbol{w}_{\text{opt}} = \boldsymbol{R}^{-1}\boldsymbol{d} \tag{3}$$

where $\boldsymbol{R}$ is the correlation matrix of the observation vector $\boldsymbol{r}$ given by

$$\boldsymbol{R} = E[\boldsymbol{r}\boldsymbol{r}^T] = E[\alpha_p^2]\boldsymbol{d}\boldsymbol{d}^T + \boldsymbol{U}E[\boldsymbol{\gamma}\boldsymbol{\gamma}^T]\boldsymbol{U}^T + \sigma^2\boldsymbol{I} \tag{4}$$

and $E[\alpha_p^2]$, the energy of the desired signature $\boldsymbol{d}$, is sum of variance $\text{var}[\alpha_p]$ and squared mean of α_p, $E[\alpha_p]^2$, i.e., $E[\alpha_p^2] = \text{var}[\alpha_p] + E[\alpha_p]^2$.

2) Minimum Variance Distortionless Response (MVDR): The basic idea behind MVDR is to impose a constraint on the response of the to be designed adaptive filter so that the desired signals will pass through the filter with a specific gain, while the output-to-interference/undesired signatures is minimized. This constrained problem can be formulated as follows:

$$\min_{\boldsymbol{w}} \boldsymbol{w}^T \boldsymbol{R} \boldsymbol{w} \text{ subject to } \boldsymbol{w}_{\text{opt}}^T \boldsymbol{d} = 1. \tag{5}$$

The solution to (5) is found by forming the Lagrangian given by $\boldsymbol{w}^T\boldsymbol{R}\boldsymbol{w} - \lambda(\boldsymbol{w}^T\boldsymbol{d} - 1)$ and solving for $\boldsymbol{w}$ as well as forming the Lagrange multiplier λ to minimize the Lagrangian. This yields the same Wiener–Hopf solution, as given in (3)

$$\boldsymbol{w}_{\text{opt}} = k_1 \boldsymbol{R}^{-1} \boldsymbol{d} \tag{6}$$

except for the constant k_1. However, this constant is not important, since both $\boldsymbol{w} = \boldsymbol{R}^{-1}\boldsymbol{d}$ and $\boldsymbol{w} = k_1\boldsymbol{R}^{-1}\boldsymbol{d}$ produce the same SINR defined in (8).

B. MSINR Approach

One widely used criteria for signal processing is the maximization of SINR. Let $\boldsymbol{R}_I$ be the correlation matrix of the interference, which consists of undesired signatures plus the noise. Namely

$$\boldsymbol{R}_I = \boldsymbol{U} E[\boldsymbol{\gamma}\boldsymbol{\gamma}^T] \boldsymbol{U}^T + \sigma^2 \boldsymbol{I}. \tag{7}$$

Therefore, the maximum SINR is defined by

$$\max_{\boldsymbol{w}} \frac{E[\alpha_p^2] \boldsymbol{w}^T \boldsymbol{d}\boldsymbol{d}^T \boldsymbol{w}}{\boldsymbol{w}^T \boldsymbol{R}_I \boldsymbol{w}} \tag{8}$$

which is equivalent to the following generalized eigenvalue problem:

$$\boldsymbol{R}_I^{-1} \boldsymbol{d}\boldsymbol{d}^T \boldsymbol{w} = \lambda_{\max} \boldsymbol{w}. \tag{9}$$

Assume that $\boldsymbol{R}$ is the correlation matrix of a random vector comprising the desired signature $\boldsymbol{d}$ and interference/undesired signatures $\boldsymbol{U}$ plus noise. Then, $\boldsymbol{R}$ is given by (4), i.e., the sum of the desired signature energy $E[\alpha_p^2]\boldsymbol{d}\boldsymbol{d}^T$ and $\boldsymbol{R}_I$. For simplicity of analysis, the desired signature $\boldsymbol{d}$ is assumed to be a one column signature vector. Extension to multiple signature vectors is straightforward.

Since $E[\alpha_p^2]\boldsymbol{d}\boldsymbol{d}^T$ is a rank-one matrix and $\boldsymbol{R}_I$ is positive definite, there is only one nonzero (and positive) eigenvalue $\lambda_{\max}$ and the optimal weight vector is given by

$$\boldsymbol{w}_{\text{SINR}} = k_2 \boldsymbol{R}_I^{-1} \boldsymbol{d} \tag{10}$$

where k_2 is a nonzero constant and the SINR is independent of the constant k_2 due to (8).

It should be noted that there is a crucial difference between the weight vector $\boldsymbol{w}_{\text{SINR}}$ in (10) and $\boldsymbol{w}_{\text{opt}}$ in (3) and (6). While the former is calculated from the correlation matrix of the interference, $\boldsymbol{R}_I^{-1}$, the latter is calculated from the correlation matrix of the observation, $\boldsymbol{R}^{-1}$.

IV. Relationship Between $\boldsymbol{R}_I^{-1}$ and $\boldsymbol{R}^{-1}$

As shown in the previous section, all three approaches generated weight vectors of the same form given by (3), (6), and (10) with different $\boldsymbol{R}_I^{-1}$ and $\boldsymbol{R}^{-1}$. This section develops the relationship between $\boldsymbol{R}_I^{-1}$ and $\boldsymbol{R}^{-1}$ that will be exploited and used in the derivation of a target signature detector in Section V.

Recalling $\boldsymbol{R}_I = \boldsymbol{U}E[\boldsymbol{\gamma}\boldsymbol{\gamma}^T]\boldsymbol{U}^T + \sigma^2\boldsymbol{I}$ given by (7), $\boldsymbol{R}$ can be reexpressed in terms of $\boldsymbol{R}_I$ and the desired signature energy as follows:

$$\boldsymbol{R} = \boldsymbol{R}_I + E[\alpha_p^2]\boldsymbol{d}\boldsymbol{d}^T. \tag{11}$$

From Woodbury's identity [16]

$$(\boldsymbol{A} + \boldsymbol{X}\boldsymbol{X}^T)^{-1} = \boldsymbol{A}^{-1} - \frac{\boldsymbol{A}^{-1}\boldsymbol{X}\boldsymbol{X}^T\boldsymbol{A}^{-1}}{1 + \boldsymbol{X}^T\boldsymbol{A}^{-1}\boldsymbol{X}} \tag{12}$$

we obtain

$$\boldsymbol{R}^{-1} = \boldsymbol{R}_I^{-1} - \frac{E[\alpha_p^2]\boldsymbol{R}_I^{-1}\boldsymbol{d}\boldsymbol{d}^T\boldsymbol{R}_I^{-1}}{1 + E[\alpha_p^2]\boldsymbol{d}^T\boldsymbol{R}_I^{-1}\boldsymbol{d}} \tag{13}$$

thus

$$\boldsymbol{R}^{-1}\boldsymbol{d} = \frac{\boldsymbol{R}_I^{-1}\boldsymbol{d}}{1 + E[\alpha_p^2]\boldsymbol{d}^T\boldsymbol{R}_I^{-1}\boldsymbol{d}}. \tag{14}$$

Equation (14) shows that $\boldsymbol{R}^{-1}\boldsymbol{d}$ and $\boldsymbol{R}_I^{-1}\boldsymbol{d}$ differ by the factor $(1 + E[\alpha_p^2]\boldsymbol{d}^T\boldsymbol{R}_I^{-1}\boldsymbol{d})^{-1}$. This factor has no effect on the choice of the weight vector $\boldsymbol{w}$ in adaptive-array processing since $\boldsymbol{w}_{\text{opt}} = \boldsymbol{R}^{-1}\boldsymbol{d}$ or $\boldsymbol{w}_{\text{SINR}} = \boldsymbol{R}_I^{-1}\boldsymbol{d}$ is scale-invariant in calculating SINR. For example, suppose that a pulse radar has a duty cycle of 0.001 and a target signal pulse occurs only 0.1% of the time. As a result, the presence of the target signal occupies such a small fraction of time that its contribution to $\boldsymbol{R}$ can be neglected. Analogous concepts are generally not true in remote-sensing imagery, which will be discussed in the following section.

V. Interpretation Orthogonal Subspace Classifier as an Adaptive Filter

The relationship between $\boldsymbol{R}_I^{-1}$ and $\boldsymbol{R}^{-1}$, described by (13) and (14) in Section IV, is important when the target signature is very weak, i.e., the energy of the target signature $E[\alpha_p^2]$ is small or $E[\alpha_p^2] \to 0$. In other words, the interference/undesired signatures dominate the target signature. In this case, it will be shown that the optimal weights given by Wiener–Hopf type solutions (3), (6), and (10) can be approximated by the same operator $\boldsymbol{q} = \boldsymbol{P}_{\text{OSP}}\boldsymbol{d}$ derived in [2]. This result is shown in the following expression (18) and has a very important implication in applications, which will be described later.

Let us first return to (11). For mathematical simplicity, we assume the undesired signature/interference to be a column vector denoted by $\boldsymbol{u}$. Then (11) can be simplified as

$$\boldsymbol{R} = \sigma^2\boldsymbol{I} + E[\alpha_u^2]\boldsymbol{u}\boldsymbol{u}^T + E[\alpha_p^2]\boldsymbol{d}\boldsymbol{d}^T \tag{15}$$

where α_u is the abundance of the undesired signature vector $\boldsymbol{u}$ and $E[\alpha_u^2]$ is the energy of $\boldsymbol{u}$ defined in the same manner as $E[\alpha_p^2]$.

Combining (3) or (6) with (15) renders

$$\begin{aligned} \boldsymbol{R}\boldsymbol{w} = \boldsymbol{d} &\Rightarrow (\sigma^2\boldsymbol{I} + \boldsymbol{u}E[\alpha_u^2]\boldsymbol{u}^T)\boldsymbol{w} = \boldsymbol{d}(1 - E[\alpha_p^2]\boldsymbol{d}^T\boldsymbol{w}) \\ &\Rightarrow \boldsymbol{R}_I\boldsymbol{w} = k_3\boldsymbol{d} \end{aligned} \tag{16}$$

where k_3 is the constant defined by $1 - E[\alpha_p^2]\boldsymbol{d}^T\boldsymbol{w}$.

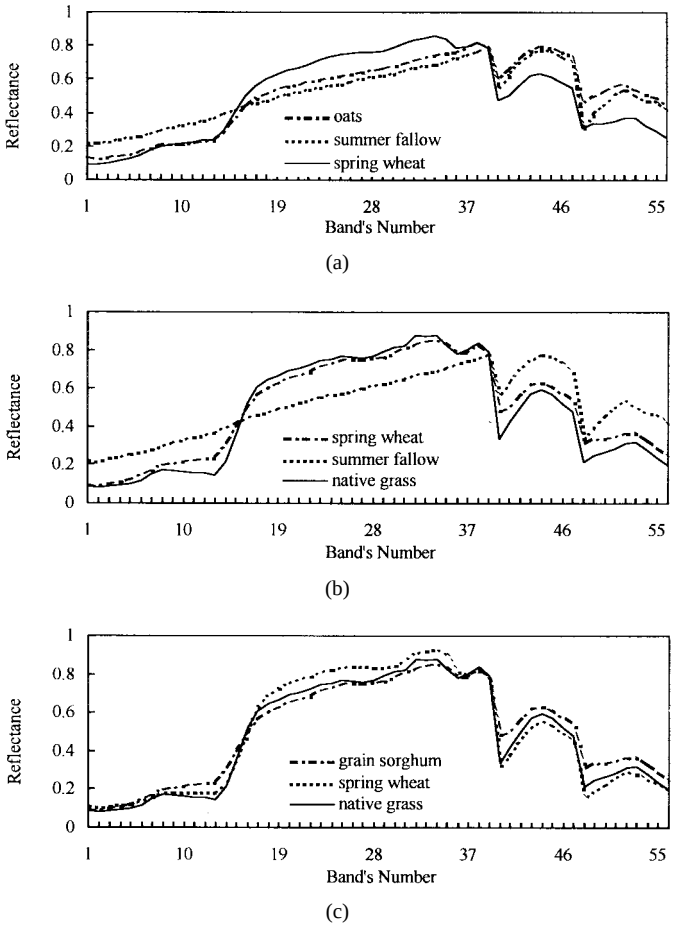

Fig. 1. (a) Reflectance spectra of data set 1, (b) reflectance spectra of data set 2, and (c) reflectance spectra of data set 3.

Applying Woodbury's identity (12) to $\boldsymbol{R}_I^{-1}$ and setting σ^2 to unity for convenience yields

$$\boldsymbol{R}_I^{-1} = I - \frac{E[\alpha_u^2]\boldsymbol{u}\boldsymbol{u}^T}{1 + E[\alpha_u^2]\boldsymbol{u}^T\boldsymbol{u}}. \tag{17}$$

If $E[\alpha_u^2] \to \infty$ (i.e., $E[\alpha_p^2] \to 0$), substituting (17) into (10) and letting $k_3 = 1$ results in

$$\boldsymbol{w}_{\text{opt}} \approx \left[\boldsymbol{I} - \frac{\boldsymbol{u}\boldsymbol{u}^T}{\boldsymbol{u}^T\boldsymbol{u}}\right]\boldsymbol{d} \tag{18}$$

which can be viewed as a projector mapping the desired signature vector $\boldsymbol{d}$ into the orthogonal complement of the space spanned by $\boldsymbol{u}$. This shows that (18) is nearly optimal when the energy of the interference/undesired signatures is very strong or, conversely, the energy of the desired signature vector is very small. If the $\boldsymbol{u}$ is replaced by an interference/undesired signature matrix to include more than a one column interference/undesired signature vector, (18) becomes

$$\boldsymbol{w}_{\text{opt}} \approx \boldsymbol{w}_{\text{SINR}} \approx [\boldsymbol{I} - \boldsymbol{U}\boldsymbol{U}^{\#}]\boldsymbol{d} \tag{19}$$

where $\boldsymbol{U}^{\#} = (\boldsymbol{U}^T\boldsymbol{U})^{-1}\boldsymbol{U}^T$ is the pseudoinverse of $\boldsymbol{U}$.

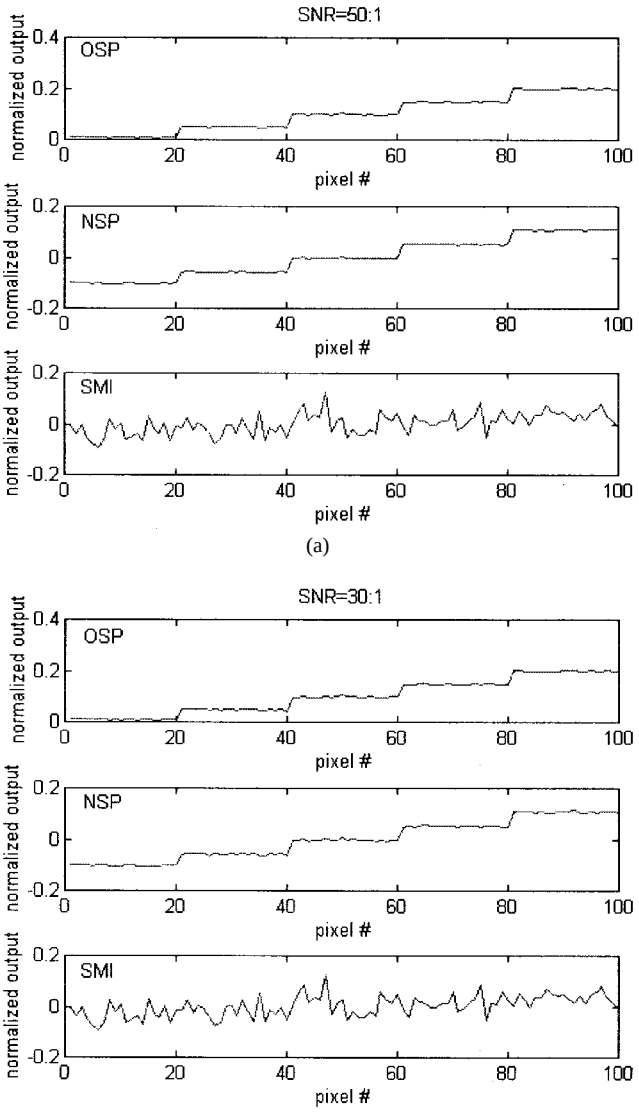

Fig. 2. Simulation results for OSP, NSP, SMI operators for data set 1: (a) normalized output versus pixel's number for SINR =50:1 and (b) normalized output versus pixel's number for SINR = 30:1.

It is not surprising to note that the right side of (19) is exactly the classifier $\boldsymbol{q} = \boldsymbol{P}_{\text{OSP}}\boldsymbol{d}$ derived in [2]. That is (19) is the OSP $\boldsymbol{P}_{\text{OSP}} = \boldsymbol{I} - \boldsymbol{U}\boldsymbol{U}^{\#}$, followed by a matched filter, based on the desired signature vector $\boldsymbol{d}$. This is obviously not a coincidence because $\boldsymbol{R} \approx \boldsymbol{R}_I$ (due to the fact that $E[\alpha_p^2] \to 0$) and the OSP approach is also based on MSINR, which results in a Wiener–Hopf-type solution. Most importantly, (19) provides an alternative view to the OSP approach: the classifier $\boldsymbol{q} = \boldsymbol{P}_{\text{OSP}}\boldsymbol{d}$ can be implemented as an adaptive filter, determined as follows by the Wiener–Hopf equation:

$$\begin{aligned}\boldsymbol{w}_{\text{opt}} &= \boldsymbol{R}^{-1}\boldsymbol{d} \approx \boldsymbol{w}_{\text{SINR}} = \boldsymbol{R}_I^{-1}\boldsymbol{d} \approx \boldsymbol{q} = \boldsymbol{P}\boldsymbol{d} \\ &= [\boldsymbol{I} - \boldsymbol{U}\boldsymbol{U}^{\#}]\boldsymbol{d}.\end{aligned} \tag{20}$$

As shown in (20), both approaches achieve nearly the same performance if the energy of the desired signature vector $\boldsymbol{d}$ is very small. However, an apparent advantage of using the optimal weight vector $\boldsymbol{w}_{\text{SINR}}$ is that it only requires knowledge of the sample correlation matrix $\boldsymbol{R}_I$ and the desired signature

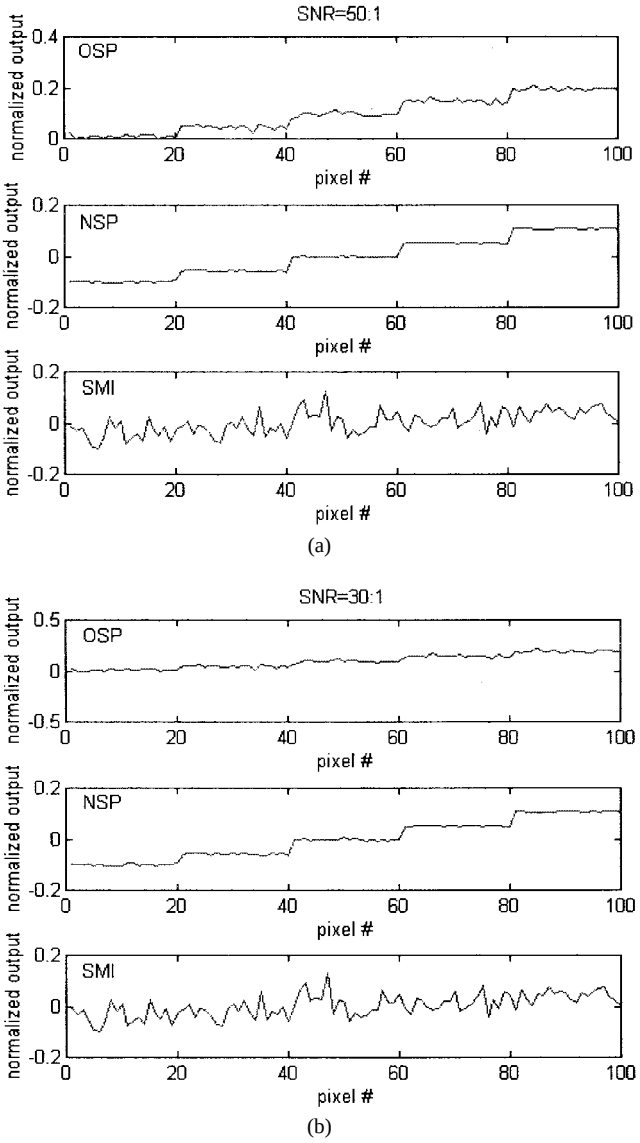

Fig. 3. Simulation results for OSP, NSP, SMI operators for data set 2: (a) normalized output versus pixel's number for SINR = 50:1 and (b) normalized output versus pixel's number for SINR = 30:1.

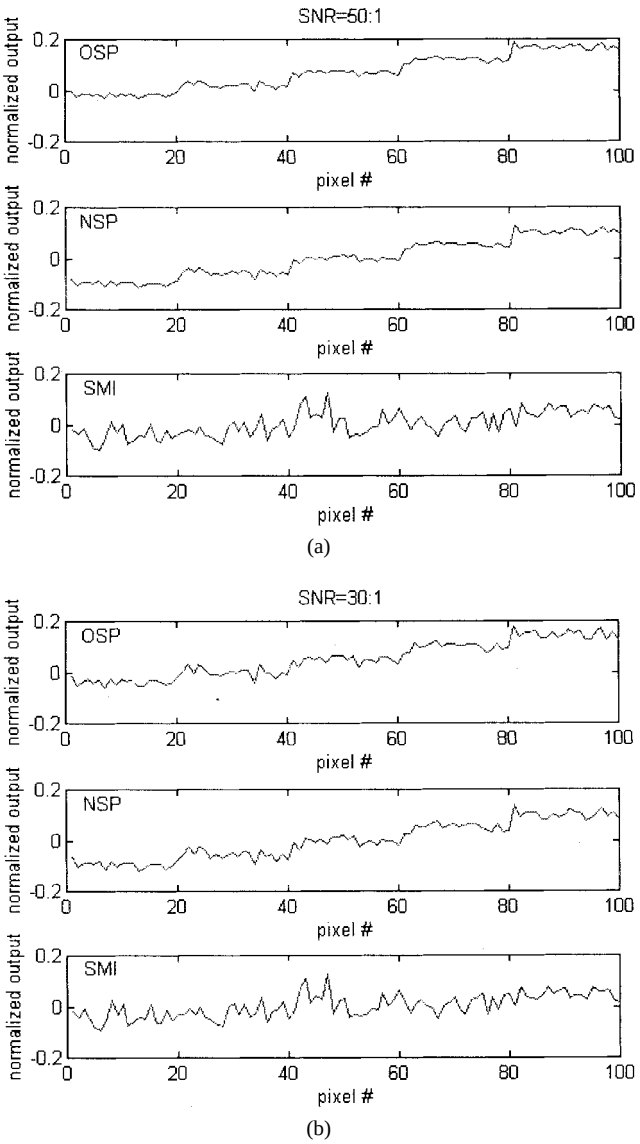

Fig. 4. Simulation results for OSP, NSP, SMI operators for data set 3: (a) normalized output versus pixel's number for SINR = 50:1 and (b) normalized output versus pixel's number for SINR = 30:1.

vector $\boldsymbol{d}$; $\boldsymbol{w}_{\mathrm{SINR}}$ does not require specific information about interference/undesired signature vectors $\boldsymbol{U}$, as are required by the OSP classifier $\boldsymbol{q}$. This advantage is particularly significant when the background is unknown and cannot be obtained *a priori*.

VI. NSP Operator

Until now, knowledge of signature vectors $\boldsymbol{M}$ including the interference/undesired signature vectors $\boldsymbol{U}$ and the desired signature vector $\boldsymbol{d}$ is assumed to be given. However, in most applications, such prior knowledge is either too expensive to collect due to the lack of samples or too difficult to obtain in practice. Under these circumstances, one must estimate the environment based on observations. In this section, the problem of target signature detection in an unknown background is considered, particularly when knowledge of signature vectors $\boldsymbol{M}$ is not necessarily given. It should be noted that $\boldsymbol{M}$ constitutes the desired signature vector $\boldsymbol{d}$ and the undesired signature vectors $\boldsymbol{U}$. Since $\boldsymbol{d}$ is the main interest and will be viewed as the target signature vector, the only information required for our problem is $\boldsymbol{d}$, not the *background*, which will be hereafter referred to as $\boldsymbol{U}$ plus the noise.

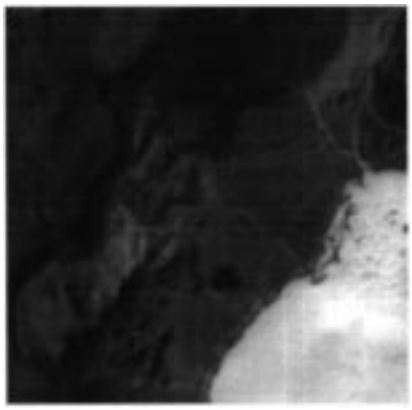

Fig. 5. A subsection of the upper left corner of the LCVF scene.

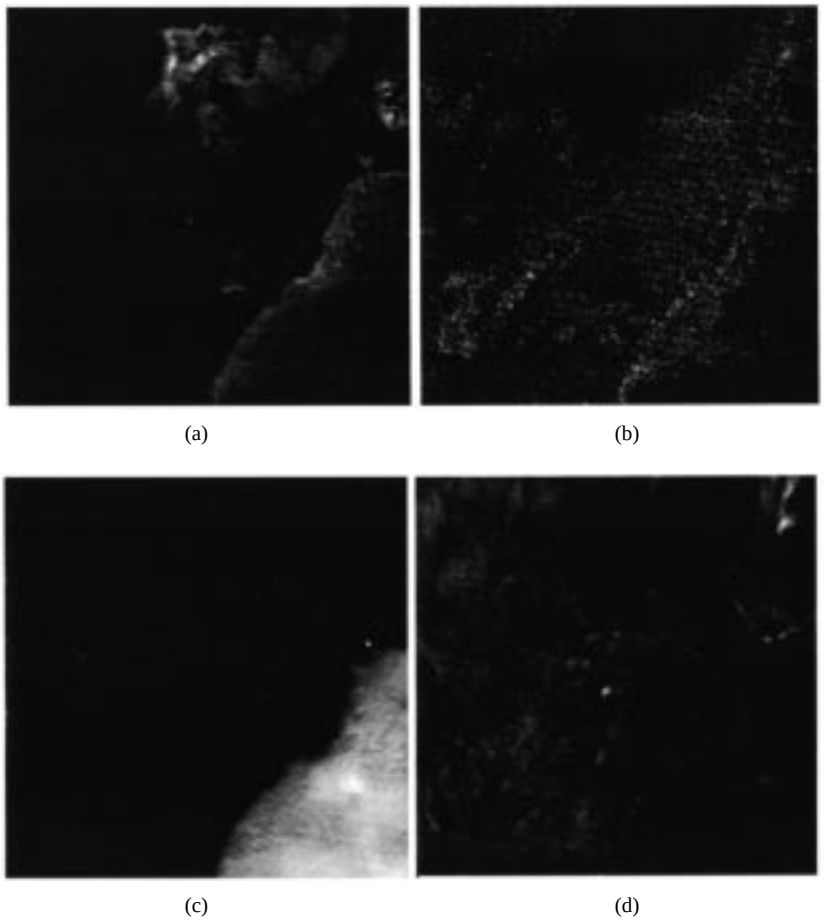

(a) (b) (c) (d)

Fig. 6. NSP method: (a) target signature is red oxidized basaltic cinders, (b) target signature is rhyolite, (c) target signature is dry playa lakebed, and (d) target signature is vegetation.

In order to estimate $\boldsymbol{d}$, we assume that knowledge of the occurrence of $\boldsymbol{d}$ is available beforehand so that $\boldsymbol{d}$ can be estimated from the pixels in the area where it resides. Let $\boldsymbol{r}$ be the observation vector made up of these pixels and $\hat{\boldsymbol{d}}(\boldsymbol{r})$ be the estimate of $\boldsymbol{d}$ based on $\boldsymbol{r}$. As defined in (4), $\boldsymbol{R}$ is the correlation matrix of $\boldsymbol{r}$ (which contains the desired signature vector $\boldsymbol{d}$) and $\boldsymbol{R}_I$, given by (7), is the correlation matrix of the background. Since $\boldsymbol{R}_I$ is nonnegative, it can be decomposed as

$$\boldsymbol{R}_I = \boldsymbol{\Phi}\boldsymbol{\Lambda}\boldsymbol{\Phi}^T = [\boldsymbol{\Phi}_I\, \boldsymbol{\Phi}_n]\begin{bmatrix}\boldsymbol{\Lambda}_I & 0\\ 0 & \boldsymbol{\Lambda}_n\end{bmatrix}[\boldsymbol{\Phi}_I\, \boldsymbol{\Phi}_n]^T \tag{21}$$

where $\boldsymbol{\Phi}$ is a matrix, whose columns are made up of eigenvectors of $\boldsymbol{R}_I$ with $\boldsymbol{\Phi}_I$ and $\boldsymbol{\Phi}_n$, corresponding to interference/undesired signature vectors $\boldsymbol{U}$ and noise $\boldsymbol{n}$, respectively. $\boldsymbol{\Lambda}_I = \text{diag}\,(\sigma_1, \sigma_2, \cdots, \sigma_m)$ with $\{\sigma_i\}_{i=1}^m = \lambda_i + \sigma^2$ and $\boldsymbol{\Lambda}_n = \text{diag}\,(\sigma_{m+1}, \sigma_{m+2}, \cdots, \sigma_l)$ with $\{\sigma_i\}_{i=m+1}^l = \sigma^2$ where $\{\sigma_j\}_{j=1}^m$ are eigenvalues of $\boldsymbol{\Phi}_I$. From (21), the inverse of $\boldsymbol{R}_I$ can be found as

$$\begin{aligned}\boldsymbol{R}_I^{-1} &= [\boldsymbol{\Phi}_I\, \boldsymbol{\Phi}_n]\begin{bmatrix}\boldsymbol{\Lambda}_I^{-1} & 0\\ 0 & \boldsymbol{\Lambda}_n^{-1}\end{bmatrix}[\boldsymbol{\Phi}_I\, \boldsymbol{\Phi}_n]^T\\ &= \boldsymbol{\Phi}_I\boldsymbol{\Lambda}_I^{-1}\boldsymbol{\Phi}_I^T + \boldsymbol{\Phi}_n\boldsymbol{\Lambda}_n^{-1}\boldsymbol{\Phi}_n^T.\end{aligned} \tag{22}$$

If the energy of the interference/undesired vectors $\boldsymbol{U}$ tends to be very large compared to the noise energy σ^2, i.e., $\lambda_i \gg \sigma^2$, then $\lambda_i^{-1} \ll \sigma^{-2}$. So, $\boldsymbol{R}_I^{-1}$ can be approximated by the second term in (22), i.e.,

$$\boldsymbol{R}_I^{-1} \approx \boldsymbol{\Phi}_n\boldsymbol{\Lambda}_n^{-1}\boldsymbol{\Phi}_n^T = \sigma^{-2}\boldsymbol{\Phi}_n\boldsymbol{\Phi}_n^T. \tag{23}$$

As a result of (23), the optimal weight vector $\boldsymbol{w}_{\text{SINR}}$ can be further approximated by

$$\boldsymbol{w}_{\text{SINR}} \approx \boldsymbol{\Phi}_n\boldsymbol{\Phi}_n^T\boldsymbol{d} = [I - \boldsymbol{\Phi}_I\boldsymbol{\Phi}_I^T]\boldsymbol{d}. \tag{24}$$

In analogy to (21), $\boldsymbol{R}$ can be written as

$$\begin{aligned}\boldsymbol{R} &= \boldsymbol{\Psi}\boldsymbol{\Gamma}\boldsymbol{\Psi}^T = [\boldsymbol{\Psi}_M\, \boldsymbol{\Psi}_n]\begin{bmatrix}\boldsymbol{\Lambda}_M & 0\\ 0 & \boldsymbol{\Lambda}_n\end{bmatrix}[\boldsymbol{\Psi}_M\, \boldsymbol{\Psi}_n]^T\\ &= \boldsymbol{\Psi}_M\boldsymbol{\Lambda}_M\boldsymbol{\Psi}_M^T + \boldsymbol{\Psi}_n\boldsymbol{\Lambda}_n\boldsymbol{\Psi}_n^T\end{aligned} \tag{25}$$

where $\boldsymbol{\Gamma} = \begin{bmatrix}\boldsymbol{\Lambda}_M & 0\\ 0 & \boldsymbol{\Lambda}_n\end{bmatrix}$. It should be noted that $\boldsymbol{\Lambda}_M$ is different from $\boldsymbol{\Lambda}_I$ in (22) because $\boldsymbol{\Lambda}_M$ is produced by both interference/undesired signature vectors and $\boldsymbol{d}$, while $\boldsymbol{\Lambda}_I$ is produced by only interference/undesired signature vectors. If the desired signature $\boldsymbol{d}$ in $\boldsymbol{R}$ is very weak, i.e., $E[\alpha_p^2]$ is very small, then

$$\boldsymbol{\Psi}_M\boldsymbol{\Lambda}_M\boldsymbol{\Psi}_M^T + \boldsymbol{\Psi}_n\boldsymbol{\Lambda}_n\boldsymbol{\Psi}_n^T \approx \boldsymbol{\Psi}_I\boldsymbol{\Lambda}_I\boldsymbol{\Psi}_I^T + \boldsymbol{\Psi}_n\boldsymbol{\Lambda}_n\boldsymbol{\Psi}_n^T \tag{26}$$

so that $\boldsymbol{R} \approx \boldsymbol{R}_I$ and $\boldsymbol{R}^{-1}$ is also approximated by

$$\boldsymbol{R}^{-1} \approx \boldsymbol{R}_I^{-1} \approx \boldsymbol{\Psi}_n\boldsymbol{\Lambda}_n^{-1}\boldsymbol{\Psi}_n^T = \sigma^{-2}\boldsymbol{\Psi}_n\boldsymbol{\Psi}_n^T. \tag{27}$$

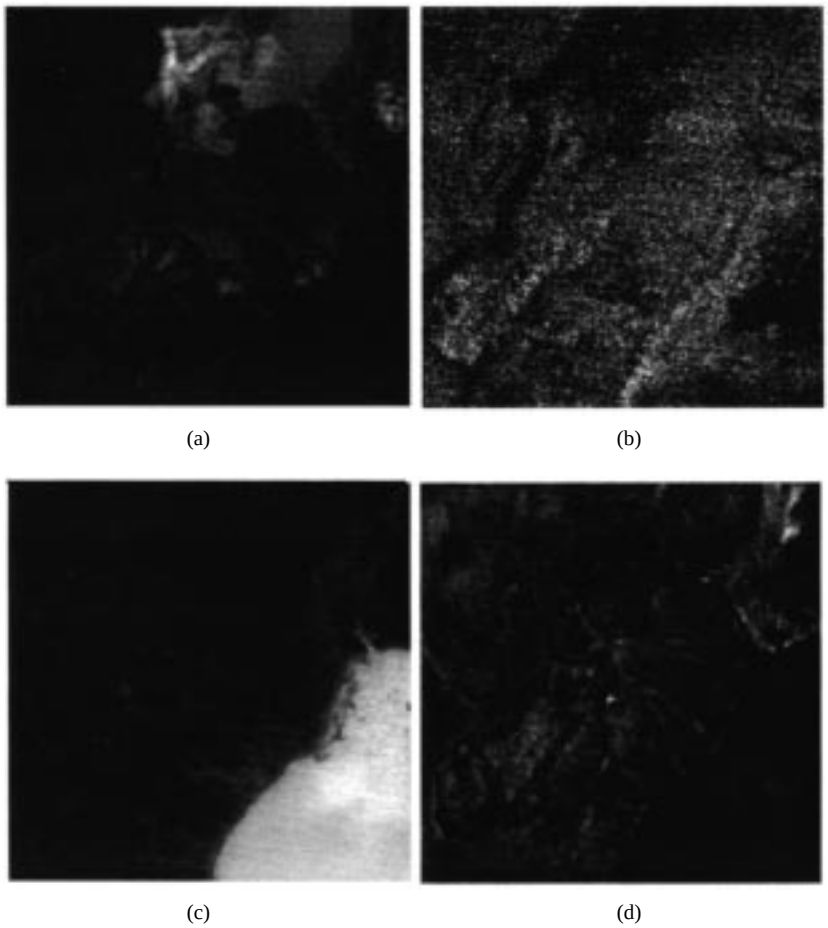

(a) (b)

(c) (d)

Fig. 7. OSP method: (a) target signature is red oxidized basaltic cinders, (b) target signature is rhyolite, (c) target signature is dry playa lakebed, and (d) target signature is vegetation.

Since both $\boldsymbol{R}$ and $\boldsymbol{R}_I$ contain the same $\boldsymbol{\Lambda}_n$, we define a new operator, the noise subspace projection operator $\boldsymbol{w}_{\mathrm{NSP}}$ by

$$\boldsymbol{w}_{\mathrm{NSP}} = \boldsymbol{\Psi}_n \boldsymbol{\Psi}_n^T \boldsymbol{d}. \tag{28}$$

An important observation can be made on (27). As shown previously, (27) is true for weak target signature vectors. However, it should be noted that (27) is also true if the energy of total signature vectors $\boldsymbol{M}$ is much larger than that of noise, i.e., $\sigma_j \gg \sigma^2$ for $j = 1, 2, \cdots, m$. In this case, $\sigma^{-2} \gg \sigma_j^{-1}$ which implies that $\boldsymbol{\Lambda}_n^{-1}$ dominates $\boldsymbol{\Lambda}_M^{-1}$ and

$$\boldsymbol{\Psi}_n \boldsymbol{\Lambda}_n^{-1} \boldsymbol{\Psi}_n^T \approx \boldsymbol{\Phi}_n \boldsymbol{\Lambda}_n^{-1} \boldsymbol{\Phi}_n^T. \tag{29}$$

As a result of (29), (28) is also true for the case of weak target signature vector as described by (26). It's worth noting that a similar idea to (29) was also proposed in [9].

In addition to the advantage that no prior information is required for signature vectors $\boldsymbol{U}$ and $\boldsymbol{d}$, two more advantages can be gained by using $\boldsymbol{w}_{\mathrm{NSP}}$ (28). One is that the detection capability of the weak target signature $\boldsymbol{d}$ can be significantly improved since the matched filter is applied after the interference/undesired signature vectors are removed. A second advantage is that no matrix inversion is needed for $\boldsymbol{w}_{\mathrm{NSP}}$. This is in contrast to adaptive filter methods that require inversion of the correlation matrix, based on the sample matrix inversion (SMI) algorithm.

In practical applications, the probability distributions governing $\boldsymbol{r}$ are not known. Consequently, the statistical correlation matrices used in the above derivations are not available but must be estimated by the sample correlation matrix $\overline{\boldsymbol{R}} = 1/N \sum_{i=1}^{N} \boldsymbol{r}_i \boldsymbol{r}_i^T$, where $\{\boldsymbol{r}_i\}_{i=1}^{N}$ is a sequence of N observation vectors. Let $y_i = \sum_{k=1}^{l} w_i r_{ik}$ be the weighted sum of the l bands in the ith observation vector $\boldsymbol{r}_i$ given by $\boldsymbol{r}_i = \boldsymbol{M}\boldsymbol{\alpha}_i + \boldsymbol{n}_i$, and where $\{\boldsymbol{n}_i\}_{i=1}^{N}$ are the noise processes. Substituting $\overline{\boldsymbol{R}}$ into (27) yields a sample version of noise subspace projection operator, $\overline{\boldsymbol{w}}_{\mathrm{NSP}}$, given by

$$\overline{\boldsymbol{w}}_{\mathrm{NSP}} = \overline{\boldsymbol{\Psi}}_n \overline{\boldsymbol{\Psi}}_n^T \boldsymbol{d}. \tag{30}$$

VII. Experimental Results

Three experiments are conducted in this section. The first experiment used computer simulations to verify the superiority of the NSP approach. The second experiment used an airborne visible infrared imaging spectrometer (AVIRIS) image to demonstrate that the classifier resulting from the NSP approach outperforms the OSP classifier in [2] and an adaptive filter using the SMI method. The third experiment shows the impressive subpixel detection capability of the NSP operator, which cannot be accomplished by the OSP operator in [2].

A. Experiment 1 (Computer Simulations)

In this experiment, we use the Field Spectrometer System (FSS) data with 60 spectral bands [17]. The major parameters

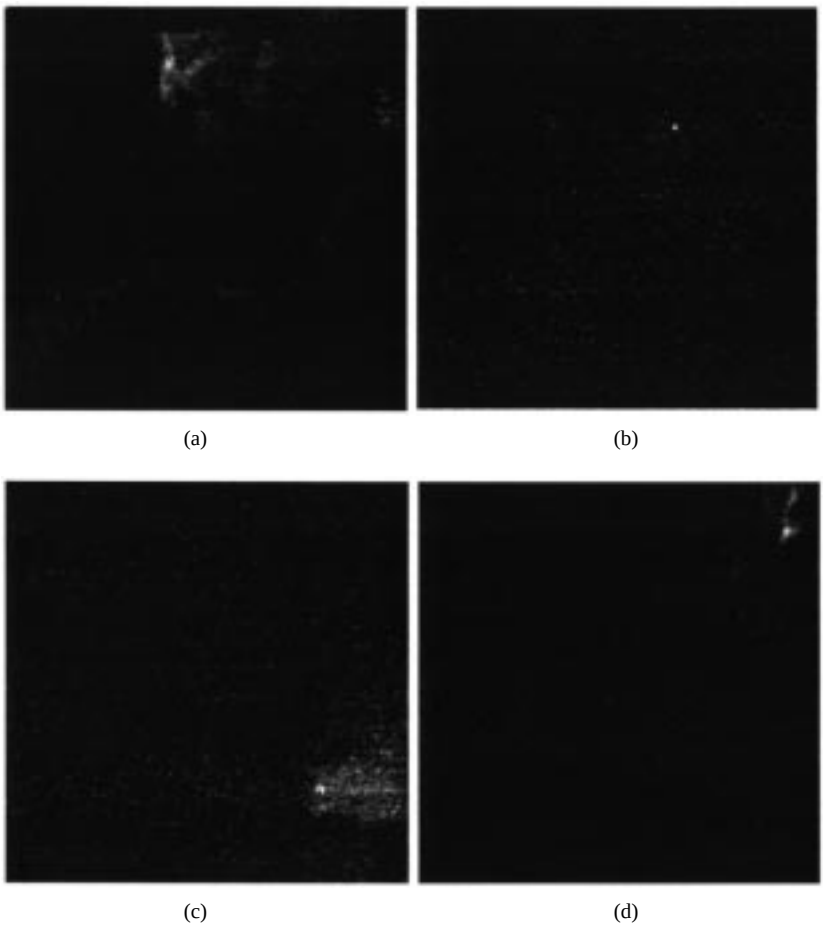

(a) (b)

(c) (d)

Fig. 8. SMI method: (a) target signature is red oxidized basaltic cinders, (b) target signature is rhyolite, (c) target signature is dry playa lakebed, and (d) target signature is vegetation.

TABLE I
PARAMETERS USED FOR FSS

Number of Bands	60 bands
Spectral Converge	0.4 - 2.4 μm
Altitude	60 m
IFOV	25 m

TABLE II
SIMULATIONS OF DESIRED AND UNDESIRED SIGNATURES FOR THREE DATA SETS

Data set	Undersired Signatures	Desired Signature
Data set-1	oats and summer fallow	spring wheat
Data set-2	spring wheat and summer fallow	native grass
Data set-3	spring wheat and grain sorghum	native grass

of the FSS data are listed in Table I. Since bands corresponding to the water absorption regions have no useful energy, they are removed prior to processing so that only 56 bands are of interest in this study. Let the number of materials $p = 3$ and $\boldsymbol{\alpha} = (\alpha_1, \alpha_2, \alpha_3)^T$ be a spectral abundance vector corresponding to a signature vector $\boldsymbol{M} = (\boldsymbol{m}_1, \boldsymbol{m}_2, \boldsymbol{m}_3)$ with $\boldsymbol{m}_3$ as the desired signature and α_3 as its associated spectral abundance. $\boldsymbol{U} = (\boldsymbol{m}_1, \boldsymbol{m}_2)$ is the undesired signature vector. Each data set contains three signatures from five materials listed in Table II. Data set 1 contains three distinct signatures, as shown in Fig. 1(a), where spring wheat is designated as the desired signature and oats, summer fallow are undesired signatures. Data set 2, shown in Fig. 1(b), contains summer fallow and two signatures with similar spectral reflectances, spring wheat and native grass with native grass selected as the desired signature. Data set 3 contains spring wheat, grain sorghum, and native grass, whose spectral reflectances are nearly indistinguishable, as shown in Fig. 1(c), with native grass chosen as the desired signature. All three data sets are simulated, based on ground truth, and 100 pixels are simulated, as given in Table III. Each pixel contains three different signatures with various spectral reflectance abundances. The 100 pixels are divided equally into five classes, each of which contains 20 pixels. The 20 pixels in each class contain the same amount of signature abundance. For example, the pixels in the first class contain 1% abundance of the desired signature and 49.5% for each of the two undesired signatures. In addition to these three signatures, three white Gaussian noises were also simulated and added to each pixel to generate two SINR's, 50:1 and 30:1, respectively, and where the SINR was the same as the SINR defined in [2].

Three methods are evaluated in this experiment.

1) The proposed NSP operator, $y = \overline{\boldsymbol{w}}_{\mathrm{NSP}}^T \boldsymbol{r}$ given by (30).
2) The OSP operator, $y = [\boldsymbol{d}^T(\boldsymbol{I} - \boldsymbol{U}\boldsymbol{U}^{\#})]\boldsymbol{r}$ given by (20).
3) The SMI method given by $y = \boldsymbol{w}_{\mathrm{opt}}^T \boldsymbol{r} = \boldsymbol{d}^T \overline{\boldsymbol{R}}^{-1} \boldsymbol{r}$.

The latter includes the calculation of direct inverting $\overline{\boldsymbol{R}}$, which is estimated from 100 samples. Figs. 2–4 are generated by

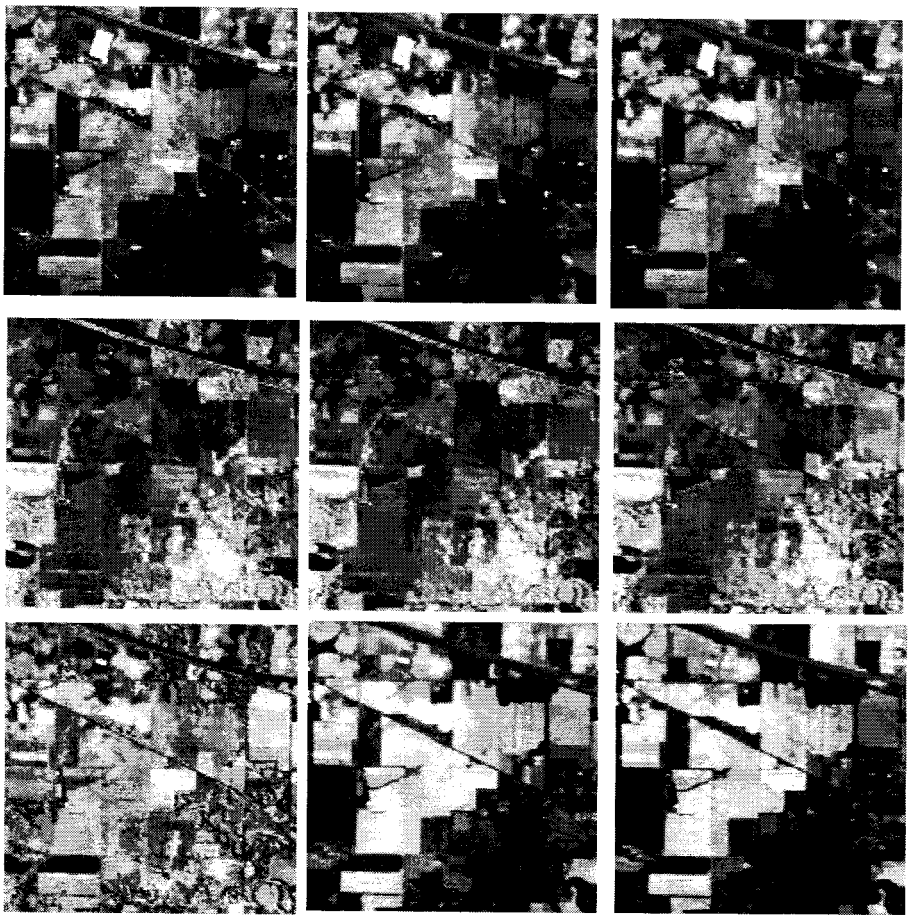

Fig. 9. Nine spectral images taken from 200 AVIRIS spectral bands (the IPTS scene) with specifications indicated in Table IV (top row: from left to right are band 8, band 16, band 27; middle row: band 39, band 46, band 70; bottom row: band 86, band 136, band 186).

TABLE III
ABUNDANCE FOR 100 SIMULATED PIXELS FOR THREE DATA SETS

Spec.\ pixel	1-20	21-40	41-60	61-80	81-100
Desired Signature	1%	5%	10%	15%	20%
Undesired Signature 1	49.5%	47.5%	45%	42.5%	40%
Undesired Signature 2	49.5%	47.5%	45%	42.5%	40%

these three methods, based on the above three data sets for SINR =50:1 and 30:1. The outputs are normalized by $y/\boldsymbol{d}^T\boldsymbol{d}$. As we can see in these figures, the SMI produced the worst performance, while the NSP operator yields the best results. It is interesting to note that unlike the OSP and SMI methods, the normalized output $y/\boldsymbol{d}^T\boldsymbol{d}$ in the NSP approach produces negative values with zero mean. This is due to the way we simulate the data sets. However, if we shift all curves by an amount, referred to as a bias calculated by the variance of the projected noise $\overline{\boldsymbol{w}}_{\mathrm{NSP}}^T\boldsymbol{n}$, the results would be similar to those produced by the OSP and SMI methods.

B. Experiment 2

In this experiment, we use the same 158-band AVIRIS data set as in [2], Fig. 5 is a subsection of this AVIRIS scene of the Lunar Crater Volcanic Field (LCVF) located in Northern Nye County, NV. Unlike [2], where the signatures were known and taken from [18], including undesired signatures, the NSP operator estimates the desired signatures from the areas in which they reside, and then the estimated signatures are used to classify various materials. In order to compare the performance of the NSP approach relative to the OSP and SMI methods, we conduct the same experiments done in [2]. Figs. 6–8 show results from the NSP, OSP, and SMI methods, respectively. The NSP generates the best results, while the SMI method produces the worst performance. Comparing Fig. 6(a)–(d) to Fig. 7(a)–(d), considerable improvements are evident, particularly in Fig. 6(a), (c), and (d), the background is cleared and the undesired signatures are nulled out. Also, the desired signatures in Fig. 6(a), (c), and (d) are more salient than those in Fig. 7(a), (c), and (d).

C. Experiment 3

The data set used in this experiment is a June 1992 AVIRIS data set of a mixed agriculture/forestry landscape in the Indian Pine Test Site (IPTS) in northwestern Indiana provided by Prof. Landgrebe and Prof. Biehl from the Purdue University School of Electrical Engineering [19]. It contains nine images, as shown in Fig. 9, of size 145 $\times$ 145 pixels from nine of the 200 spectral bands, as indicated in Table IV. Fig. 10 is a map, which provides the ground truth of Fig. 9. As we can see in Fig. 9, the United States Highways 52 and 231 in the top of the right corner are barely visible. Three additional roads (one is across the top from east to west, another is a

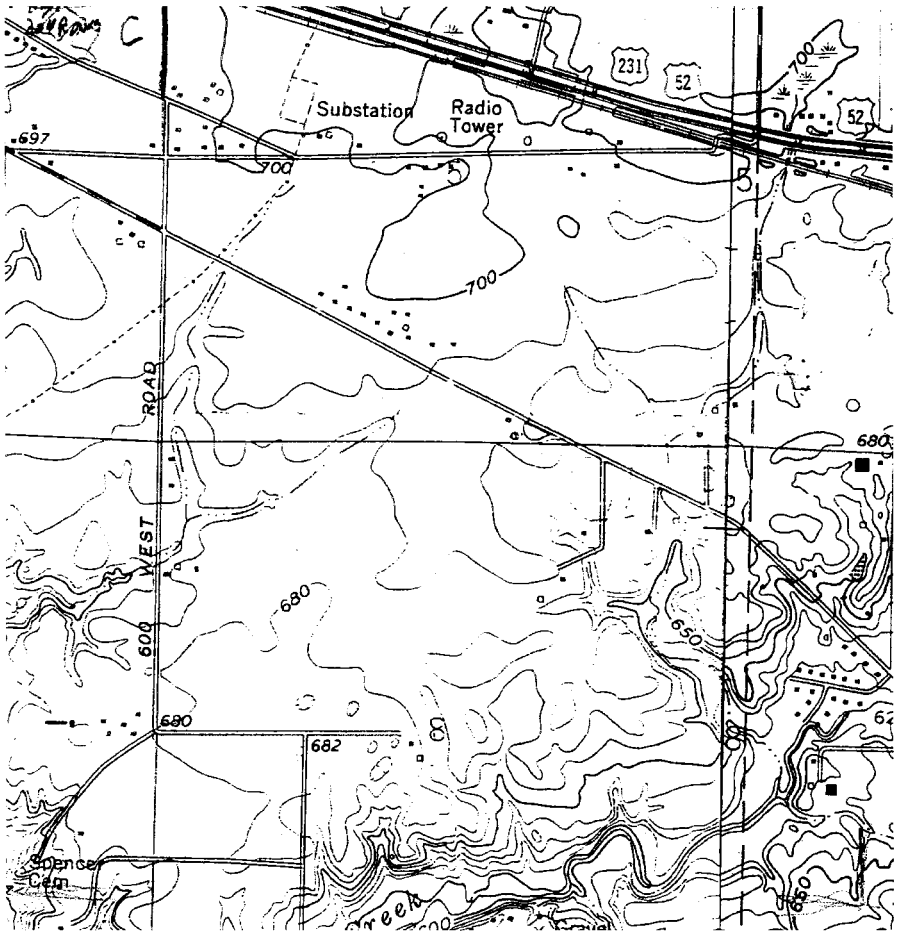

Fig. 10. Portion of a USGS Quadrangle map of the IPTS scene.

TABLE IV
THE BAND DESCRIPTION OF THE EXPERIMENT 3

AVIRIS Band #.	Wavelength center, *um*
8	0.4795
16	0.5584
27	0.6675
39	0.7560
46	0.8235
70	1.0550
86	1.2092
136	1.6589
186	2.2186

Fig. 11. Image resulting from the NSP operator.

north–southbound West Road, and the third road crosses from southeast to northwest) are almost invisible in the image.

Since there is no prior knowledge of the signatures of roads and the background available from the image in Fig. 9, the OSP method cannot be applied. However, estimates of the signatures of these three roads are possible. For this example, we select six pixels from a visible portion of the road across from east to west, then find these six corresponding pixels in all nine bands and average them. The averaged six pixels were used as the estimate of the desired target signature for Highways 52, 231, and the three roads. Finally, the NSP operator (30) was applied to the image in Fig. 9 to produce the image given by Fig. 11. This image clearly shows the two highways and three roads. In this experiment, it was noted that a road near the right boundary of the image in Fig. 11, which connects the United States highways and the country road across from southeast to northwest is picked up in Fig. 11, but is not visible in Fig. 9 nor shown in the map (Fig. 10). However, it does exist when we examine all nine spectral images in Fig. 9 carefully. The selection of pixels to estimate the desired signatures is not unique. Several areas, for example, areas on the north–southbound west road and the road crossing from southeast to northwest, were tried and produced nearly the same results.

In addition to extracting roads, some other areas with the same estimated signature are also extracted in the image, such as a substation shown in the top of the left corner.

This experiment demonstrates a potential application of the proposed NSP approach for the detection of weak target signatures in an unknown background.

VIII. Conclusion

In this paper, a noise subspace projection (NSP) is presented. The resultant NSP operator can be designed as a classifier or a subpixel detector to detect and extract target signatures in an unknown background. The advantages of the NSP operator are 1) that no prior knowledge of signatures and background is required and 2) implementation does not require matrix inversion. The former can be estimated from observations and the latter is done by simply inverting the eigenvalues of the correlation matrix. The proposed NSP approach offers an attractive alternative method for subpixel target detection and scene pixel classification in high data dimensionality, hyperspectral imagery.

Acknowledgment

The authors would like to thank Prof. D. A. Landgrebe of Purdue University for providing the FSS data and the AVIRIS data set of the Indian Pine Test Site. We also thank Dr. C. Harsanyi for providing the AVIRIS data of the Lunar Crater Volcanic Field. We also want to express our appreciation for the anonymous reviewers' suggestions, which greatly improved this paper's quality and presentation.

References

[1] G. Vane and A. F. H. Goetz, "Terrestrial imaging spectroscopy," *Remote Sens. Environ.*, vol. 24, no. 1, pp. 1–29, 1988.
[2] C. Harsanyi and C.-I. Chang, "Hyperspectral image classification and dimensionality reduction: An orthogonal subspace projection approach," *IEEE Trans. Geosci. Remote Sensing*, vol. 32, pp. 779–785, July 1994.
[3] Zhao, "Subspace projection approach to hyperspectral image classification using linear spectral mixture model," M.S. thesis, Dept. Comput. Sci. Elect. Eng., Univ. Maryland-Baltimore County, May 1996.
[4] T.-M. Tu, C.-H. Chen, and C.-I. Chang, "*A posteriori* least squares orthogonal subspace projection approach to desired signature extraction and detection," *IEEE Trans. Geosci. Remote Sensing*, vol. 35, pp. 127–139, Jan. 1997.
[5] C.-I. Chang, "Error analysis of least squares subspace projection approach to linear mixing problems," to be published.
[6] T.-M. Tu *et al.*, "An oblique subspace projection approach to mixed pixel classification in multispectral/hyperspectral images," to be published.
[7] J. Settle, "On the relationship between spectral unmixing and subspace projection," *IEEE Trans. Geosci. Remote Sensing*, vol. 34, pp. 1045–1046, July 1996.
[8] J. C. Harsanyi, "Detection and classification of subpixel spectral signatures in hyperspectral image sequences," Ph.D. dissertation, Dept. Elect. Eng., Univ. Maryland-Baltimore County, Aug. 1993.
[9] H. Subbaram and K. Abend, "Interference suppression via orthogonal projections: A performance analysis," *IEEE Trans. Antennas Propagat.*, vol. 41, pp. 1187–1193, Sept. 1994.
[10] J. B. Adams and M. O. Smith, "Spectral mixture modeling: A new analysis of rock and soil types at the Viking Lander 1 site," *J. Geophys. Res.*, vol. 91, pp. 8098–8112, July 1986.
[11] Y. E. Shimabukuro and J. A. Smith, "Least squares mixing models to generate fraction images derived from multispectral data," *IEEE Trans. Geosci. Remote Sensing*, vol. 29, pp. 16–20, Jan. 1991.
[12] A. R. Gillespie, M. O. Smith, J. B. Willis, S. C. Fischer, A. F. III, and D. E. Sabol, "Interpretation of residual images: Spectral mixture analysis of AVIRIS images," in *Proc. 2nd AVIRIS Workshop*, Owens Valley, CA, JPL Publ. 4/5, June 1990, pp. 243–270.
[13] B. D. Van Veen and K. M. Buckley, "Beamforming: A versatile approach to spatial filtering," *IEEE ASSP Mag.*, pp. 4–24, Apr. 1988.
[14] J. E. Hudson, *Adaptive Array Principles.* London, U.K.: Peregrinus, 1981.
[15] S. Haykin, *Advances in Spectrum Analysis and Array Processing, Vol. 2.* Englewood Cliffs, NJ: Prentice-Hall, 1991.
[16] L. Scharf, *Statistical Signal Processing: Detection, Estimation, and Time Series Analysis.* Reading, MA: Addison-Wesley, 1991.
[17] L. L. Biehl *et al.*, "A crops and soils data base for scene radiation research," in *Proc. Machine Processing Remotely Sensed Data Symp.*, 1982, pp. 169–177.
[18] W. H. Farrand and R. B. Singer, "Analysis of altered volcanic pyroclasts using AVIRIS data," in *Proc. Third AVIRIS Workshop*, Pasadena, CA, 1991, JPL Publ. 91-28.
[19] D. A. Landgrebe and L. L. Biehl, *An Introduction to MultiSpec*, School Elect. Eng., Purdue Univ., West Lafayette, IN, 1995.

Te-Ming Tu was born in Kaohsiung, Taiwan, R.O.C., in 1959. He received the B.S.E.E. degree from Chung Cheng Institute of Technology, Taoyuan, Taiwan, in 1986, the M.S.E.E. degree from National Sun Yat-Sen University in 1991, and the Ph.D. degree in electrical engineering from the National Cheng Kung University, Tainan, Taiwan, in 1996.

Since 1981, he has been employed by the R.O.C. Army Command, working on communication engineering. He was a Teaching Assistant from 1986 to 1989, an Instructor from 1991 to 1993, and is currently an Associate Professor in the Department of Electrical Engineering, Chung Cheng Institute of Technology. His research interests include remote sensing, medical imaging, neural networks, and statistical pattern recognition.

Chin-Hsing Chen was born in Tainan, Taiwan, R.O.C., in 1958. He studied at National Taiwan University, Taipei, where he received the B.S. degree in electrical engineering in 1980. After serving as a communication officer in the Chinese Marine Corps for two years, he returned to graduate studies at the University of California, Santa Barbara (UCSB), where he worked on research projects joined by the Santa Barbara Research Center and Delco Electronics. He received the M.S. and Ph.D. degrees in electrical and computer engineering from UCSB in 1983 and 1987, respectively.

He was an Associate Professor from 1988 to 1996 and is currently a Professor in the Department of Electrical Engineering, National Cheng Kung University, Tainan. His current interests include medical imaging, remote sensing, robot vision, fractal and chaos, wavelet transform, and systolic circuit implementation.

Chein-I Chang (S'81–M'82–SM'92) received the B.S. degree from Soochow University, Taipei, Taiwan, R.O.C., in 1973, the M.S. degree from National Tsing Hua University, Hsinchu, Taiwan, in 1975, and the M.A. degree from the State University of New York at Stony Brook, in 1977, respectively, all in mathematics. He also received the M.S. and M.S.E.E. degrees from the University of Illinois, Urbana-Champaign, in 1980 and 1982, respectively, and the Ph.D. degree in electrical engineering from the University of Maryland, College Park, in 1987.

He was a Visiting Assistant Professor from January 1987 to August 1987, Assistant Professor from 1987 to 1993, and is currently an Associate Professor in the Department of Computer Science and Electrical Engineering, University of Maryland-Baltimore County. He was a Visiting Specialist in the Institute of Information Engineering at National Cheng Kung University, Tainan, Taiwan, from 1994 to 1995. His research interests include information theory and coding, signal detection and estimation, multispectral/hyperspectral remote sensing, neural networks, and pattern recognition.

Dr. Chang is a member of SPIE, INNS, Phi Kappa Phi, and Eta Kappa Nu.